Senior Honors Thesis:

Thermal Fabrication of Gold Nanocages

Miroslav Remec

April 20, 2011

Professor James Dickerson
PHYS 296B Honors Research

Abstract

The purpose of this research project was to test and characterize a new method for gold nanoparticle production. The main idea was based on the preliminary observations made in earlier work, which had suggested that small amounts of gold deposited onto a silicon substrate will spontaneously reshape into gold nanoparticles when treated to controlled high-temperature heating for a sufficient period of time. This idea for a fabrication process was extended to incorporate Electron Beam Lithography (EBL) gold patterning. The full fabrication method consisted of the following steps: (1) Preparation of clean silicon substrates, (2) Addition of a Poly(methyl methacrylate) (PMMA) Coat via spin coating, (3) Design of gold patterns for the EBL, (4) Gold patterning via EBL, (5) Gold deposition via electron beam evaporation, (6) PMMA mask removal via acetone wash, and (7) High-Temperature furnace heating, as well as plans for a final step (8) Isolation of the gold nanocages via HF etching. The project research required the use of the photolithographic facilities of the Vanderbilt Institute of Nanoscale Science and Engineering (VINSE), as well as the use of the high-temperature furnace and other basic needs supplied by the research group of Professor Dickerson. Some of the VINSE equipment required relatively extensive operational training.

The research project has demonstrated that the described thermal fabrication method can uniformly and repeatedly produce Au nanoparticles of about 400 nm in diameter from Au deposits of 1 um^2 area and 20 nm thickness. Larger areas displayed structural fragmentation into multiple nanoparticles, and this fragmentation effect increased proportionally with increasing area size. Due to time constraints, the many available parameters prevented a complete characterization of this fabrication method; however, useful insights were obtained for several of the parameters of the fabrication process. In particular, it can be expected that smaller nanoparticles may be fabricated in a straightforward manner by reducing the patterned area sizes of the gold deposits. Results suggested an intrinsic limitation to the method: for the requirement of product uniformity, each Au-area deposit had to produce only a single nanoparticle.

Table of Contents

1.0 Introduction

1.1 A brief review of the theory of nanoparticle interactions with electromagnetic waves

One interesting property of metal nanoparticles (NPs) is their response to electromagnetic waves. Long before the underlying physical theory was even formulated - far less understood - ancient artisans were adding colloidal gold to glass in order to produce the brilliant colors of stained glasses. One such cultural treasure is the rose window of the Notre Dame Cathedral in Paris, France, completed circa 1225 (Fig. 1).

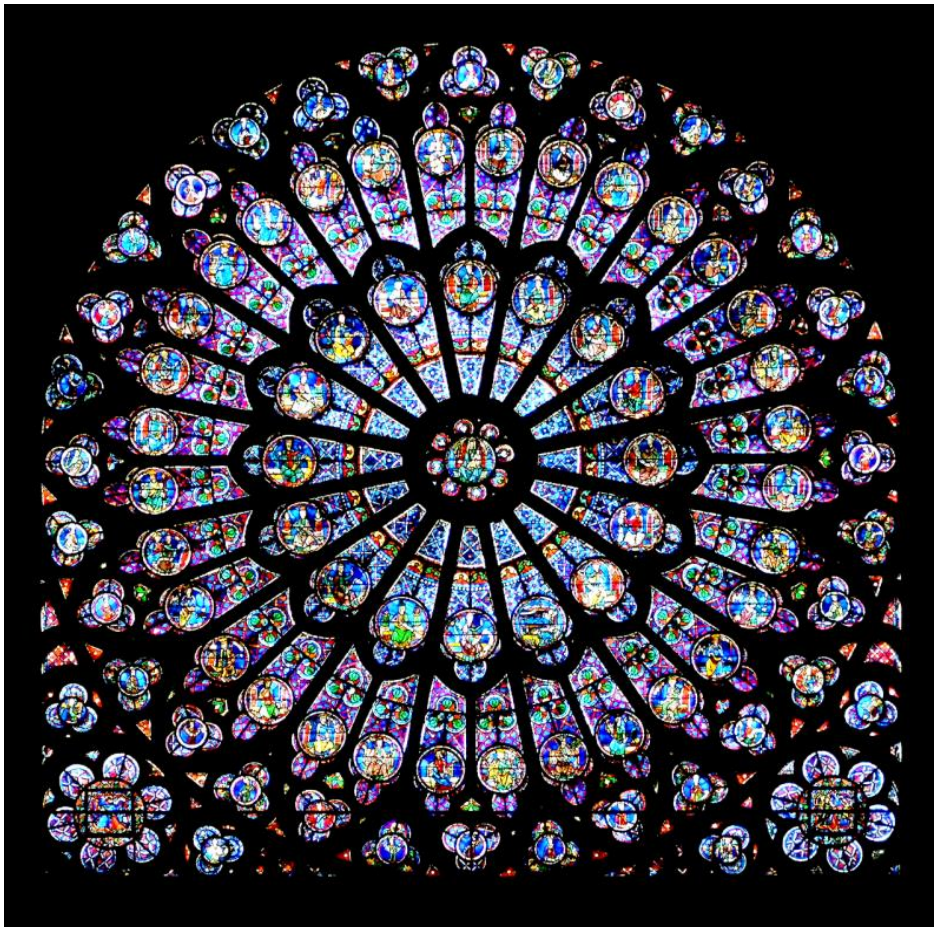

Fig. 1: Stained glass rose window of Notre Dame de Paris; completed circa 1225.

In 1908, the German physicist Gustav Mie published his canonical paper on the simulation of the color changes in colloidal gold particles, using the classical Maxwell theory of electromagnetism.[1] In his paper, he demonstrated the computation of light scattering by small dielectric spheres (20 – 1600 nm), and his work explained how different sizes of gold particles in a colloidal solution can account for the different colors of the solutions. For the case of fine metal suspensions in which these particles are small in size with respect to both the incident wavelengths and the separation distances between them, this theory produces a well-defined absorption curve characterized by a resonance-like shape. Mie concluded that the observed properties of the gold colloidal solutions can be explained by an interaction of two distinct properties of the gold particles: (1) a sharp maximum in absorption of green light, and (2) a maximum in reflection of yellow-red light. Smaller particles reflect only weakly and absorb strongly; consequently the solution displays a ruby red color. Larger particles reflect more strongly and absorb more weakly; so the solution displays a bluer color. This dual interaction means that the precise manipulation of the NP size distribution is enough to display any possible color of the visible spectrum in a solution of gold colloids.

Details are illustrated below (Fig. 2).[1] For small particles ($d = 2r < 40$ nm), light absorption dominates the resonance peak, which lies in the wavelength range 510 – 530 nm (green). Thus, the solution is ruby red (the color complementary to green). With increasing particle size, the resonance peak heightens and shifts towards longer wavelengths. The most pronounced resonance appears at a sphere diameter of ~ 80 nm for a wavelength of ~ 560 nm (yellow-green), where the solution is purple. For larger spheres, the resonance peak continues to move toward longer wavelengths, but its maximum also decreases rapidly. For spheres of 140 nm radius, this broad absorption peak crests at ~ 620 nm; the solution appears blue.

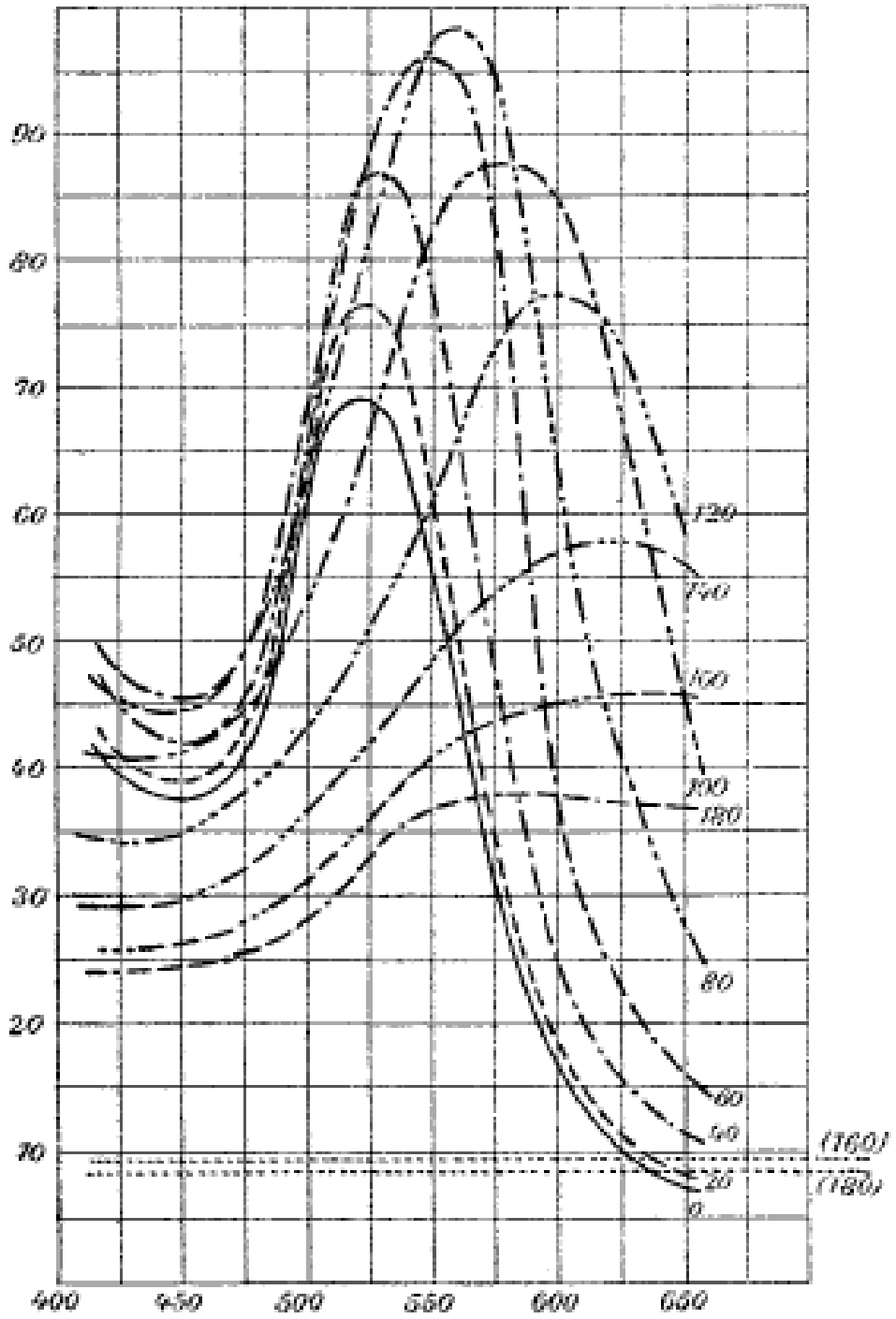

Fig. 25. Absorption kolloidaler Goldlösungen.

Fig. 2: Absorption of colloidal gold solutions. Light loss (in units per thousand) on a 1 mm path through a solution of [Au] = 10^{-6} M (1 mm^3 Au in 1 L water) vs. wavelength (i.e. 80 = 8% light loss per 1 mm travel).[1] The predictions of Mie theory have been compared with experimental results, such as in a recent effort undertaken at Rice University (Fig. 3).[2] Five gold NP samples were selected, with average diameters from 51 to 237 nm. This range span was intentional, such that the absorption dominates the contribution to extinction at the smaller sizes, while the scattering dominates at the larger sizes. These differences are seen in the calculated spectra of scattering and absorption as shown in the right column (Fig. 3).[2] Each of the samples was characterized by ensemble extinction spectroscopy and scanning electron microscopy (SEM). For each sample, an insert in the left panel shows the size distribution of the NPs in the sample. The data of the two columns suggest that the agreement between theory and experiment is excellent.

Other than Mie theory, diverse methods have been profitably developed to calculate the absorption and scattering spectra of similar NPs in solid matrices, colloidal solutions, and suspensions of nanoshells. The T-matrix methods, discrete dipole approximation (DDA), the Maxwell-Garnett effective medium approximation (EMA), and others have all produced satisfactory agreement with experimental results.[3, 4]

For example, another theoretical derivation of the resonance behavior for the scattering and absorption cross sections of Au spheres embedded in a dielectric matrix is displayed below, this time derived by the Maxwell-Garnett EMA (Fig. 4).[4] These results provide conclusions consistent with earlier observations. First, the wavelength of the resonance peak depends on the size of the nanospheres: for spheres of 5 nm radius, it occurs at ~ 550 nm, while for spheres of 15 nm radius, it occurs at ~ 620 nm. Second, the smaller spheres display a resonance dominated by the absorption contribution, while the larger spheres display resonance behavior where the scattering and absorption factors have about equal contribution.

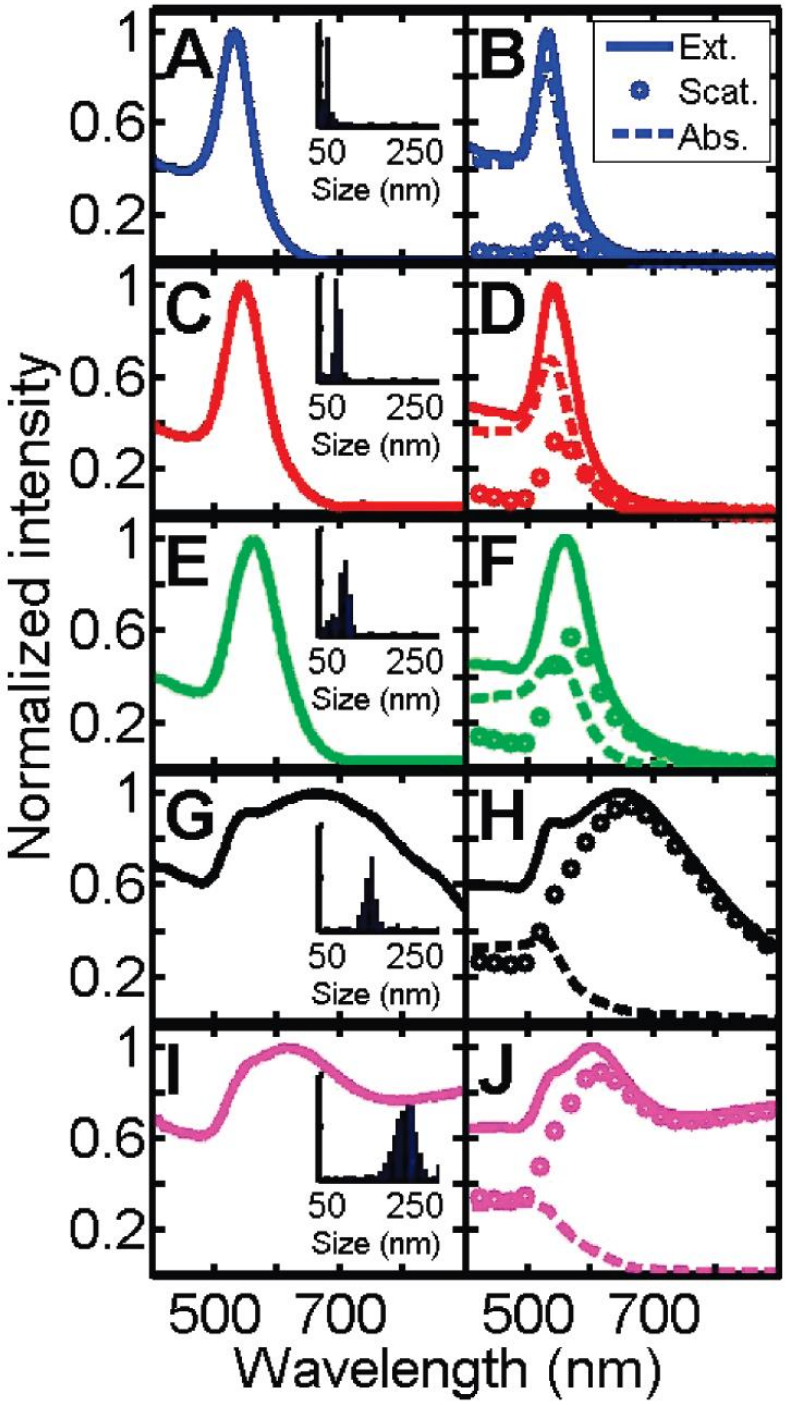

Fig. 3: Experimental extinction spectra (left column) and Mie theory spectra (right) for spherical gold NPs with different mean sizes: A, B 51 nm; C, D, 76 nm; E, F, 88 nm; G, H, 155nm; and I, J, 273 nm. The Mie theory spectra (solid lines) can be separated into scattering (open circles) and absorption (dashed lines).[2]

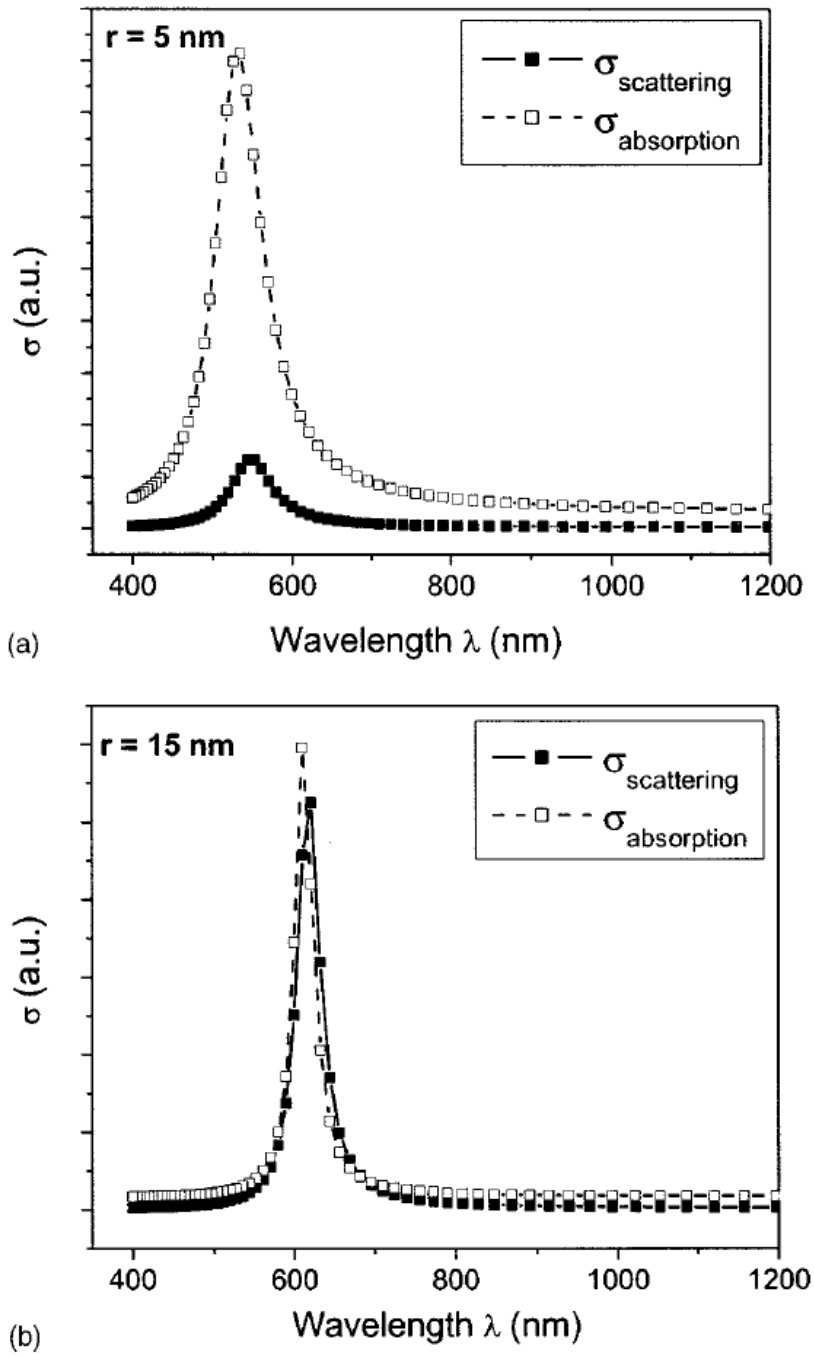

Fig. 4: Calculated scattering (σ_{sca}) and absorption (σ_{abs}) cross sections for gold nanospheres with diameters d = 10 nm (a) and d = 30 nm (b), as derived from the theory of Maxwell-Garrett EMA. [4]

For the case where the radius R of a spherical nanoparticle is much smaller than the wavelength λ of the impinging wave, Mie theory yields a simple expression for the particle extinction cross section σ_{ext}, with ε_m as the dielectric function of the medium (i.e., water) and $\varepsilon(\omega) = \varepsilon_1(\omega) + i\,\varepsilon_2(\omega)$ as the (complex) dielectric function of the cluster (sphere), which itself depends on the frequency of the impinging wave[5]:

$$\sigma_{ext} = \frac{24\,\pi^2 R^3 \varepsilon_m^{\frac{3}{2}}}{\lambda} \frac{\varepsilon_2(\omega)}{[\varepsilon_1(\omega) + 2\varepsilon_m]^2 + \varepsilon_2(\omega)^2}$$

The spectral features of the extinction cross section – that is, the position and shape of the resonance peak – depend indirectly on the radius R, through the dependence of the $\varepsilon(\omega)$ dielectric function on the particle size. From the equation, it is clear that the cross section exhibits a maximum resonance when $\varepsilon_1(\omega) = -2\varepsilon_m$, provided that the $\varepsilon_2(\omega)$ term is small or relatively constant in the vicinity of resonance.

So it is clear how Mie theory divides the problem into two parts: the scattering of the electromagnetic wave is derived from first principles (by Maxwell's equations), yet the characteristic material properties are treated phenomenologically with the introduction of material dielectric functions. These functions may differ from those of the bulk material, so as to incorporate all of the property effects distinct to the cluster, to give rise to a spectral response as is observed experimentally. Mie theory is restricted to this phenomenological character: it cannot analyze the motion of electrons, or their discrete energy states.[5]

The extinction cross section σ_{ext} equals a sum of the absorption σ_{abs} and scattering σ_{sca} cross sections:

$$\sigma_{ext} = \sigma_{abs} + \sigma_{sca}$$

At the SPR resonance, the cross sections of the gold nanoparticles can be much larger than those of traditional dyes. For example, gold nanocages of 45 nm edge length and 3.5 nm wall thickness (and 25% residual silver alloyed with the gold) with an SPR peak around 810 nm exhibit σ_{abs} = 3.48 x 10^{-14} m^2 and σ_{sca} = 1.41 x 10^{-14} m^2, both of which are several orders of magnitude higher than the cross sections of traditional organic dyes, such as Indocyanine Green, which exhibits σ_{abs} = 2.9 x 10^{-20} m^2 at 800 nm.[6, 7]

The intensity of a parallel beam of incident light exponentially attenuates through the medium due to absorption (which generates heat) and scattering (which changes the direction of light propagation). This attenuation caused by nanoparticles can be expressed in terms of the extinction cross section, with $I(z=0)$ and $I(z)$ denoting the intensity of the wave on the surface and at a depth z in the medium respectfully, and with n denoting the particle number density (i.e., the number of particles per volume):

$$I(z) = I(z=0)e^{-n\sigma_{ext}z} = I(z=0)e^{-n\sigma_{abs}z}e^{-n\sigma_{sca}z}$$

A typical value of particle density (57 µg / mL) used in measurements of the optical properties of Au NP suspensions is analyzed below, to quantify a required number of nanoparticles for suspension (Table 1).[3]

Table 1: Amounts of solid Au nanospheres for a suspension with [Au] = 57 µg / mL (Au ρ = 19.30 g*cm^{-3}).

NP Radius	NP Surface Area	NP Volume	Single NP Mass	Number of NPs	Number of NPs
r	$4\pi r^2$	$(4/3)\eth r^3$	V x ρ	1 µg / [NP mass]	[# NP per µg] x [Au]
(nm)	$(nm)^2$	$(nm)^3$	(µg)	(per µg gold)	(per mL solution)
10	1.26E+03	4.19E+03	8.08E-11	1.24E+10	7.05E+11
20	5.03E+03	3.35E+04	6.47E-10	1.55E+09	8.81E+10
30	1.13E+04	1.13E+05	2.18E-09	4.58E+08	2.61E+10
40	2.01E+04	2.68E+05	5.17E-09	1.93E+08	1.10E+10
50	3.14E+04	5.24E+05	1.01E-08	9.90E+07	5.64E+09
60	4.52E+04	9.05E+05	1.75E-08	5.73E+07	3.26E+09
70	6.16E+04	1.44E+06	2.77E-08	3.61E+07	2.06E+09

80	8.04E+04	2.14E+06	4.14E-08	2.42E+07	1.38E+09
90	1.02E+05	3.05E+06	5.89E-08	1.70E+07	9.67E+08
100	1.26E+05	4.19E+06	8.08E-08	1.24E+07	7.05E+08
168	3.55E+05	1.99E+07	3.83E-07	2.61E+06	1.49E+08
200	5.03E+05	3.35E+07	6.47E-07	1.55E+06	8.81E+07
212	5.65E+05	3.99E+07	7.70E-07	1.30E+06	7.40E+07
300	1.13E+06	1.13E+08	2.18E-06	4.58E+05	2.61E+07

Now, in order to elaborate a microscopic theory of the interaction of electromagnetic waves with metal NPs, we start simply with the fact that when placed in an external electric field, the distribution of free electrons in a metal will move relative to the distribution of positive ions in order to cancel the electric field within it. If the external electric field is oscillating, it will cause the electron density of the metal to oscillate as well. The rapid oscillations of free electrons in conducting media such as plasmas or metals are known as plasma oscillations (Langmuir waves). In the world of quantum mechanics, quantization of these plasma oscillations leads to quasiparticles named plasmons, as quantization of electromagnetic fields leads to photons and that of mechanical vibrations leads to phonons. When the metal objects are small compared to the incident wavelength, on the order of the nanoscale (to a few hundred nm radius), the plasmon phase space is reduced. Then, light-induced plasmon oscillations on the incident surfaces of the NPs come to exhibit a particular resonance-like behavior, called surface plasmon resonance (SPR). A simple concept of the phenomenon is shown below, with incident light and plasmon oscillations (Fig. 6).[8]

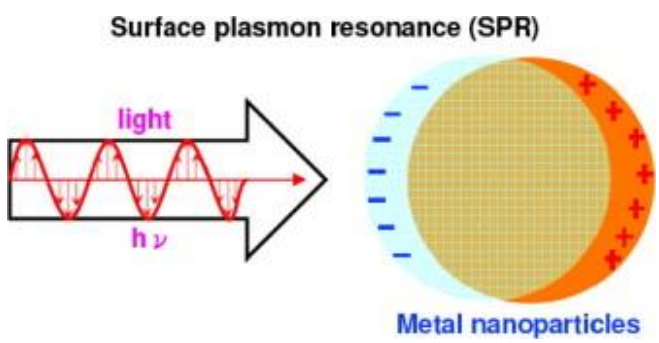

Fig. 6: The schematic of the phenomenon of surface plasmon resonance (SPR) for metal nanoparticles. [8]

It has been shown that the wavelength at which SPR occurs depends not only on the size of the NPs, but also on the structural shape, the degree of particle-to-particle coupling, the properties of the metal and substrate with which the NPs are made, and the dielectric properties of the surrounding matrix in which the NPs are embedded.[8, 9] Thus, variation of these parameters through precise control of the fabrication process can tune the SPR peak to any desired wavelength. This opens doors to a number of applications.

1.2 A brief review of the applications of Au nanoparticles and the uses of its electromagnetic effects

The field of nanoscience was perhaps first set out by Richard Feynman, who as early as 1959 argued the benefits and even necessity of expanding fundamental science to the smaller size scale in his famed talk, "There's Plenty of Room at the Bottom!"[10] In general, the nanoscale can reveal fascinating features for any material, due to the significantly larger surface-to-volume ratios at the nanoscale compared to the material in bulk, which means key physical properties may differ greatly from those of bulk materials.[5] Due to the small size, biocompatible nanomaterials may enter biological cells *in vivo*, and agents chemically attached to these material surface can target their bonding for high specificity (i.e., "surface functionality"). Resonant SPR effects are exhibited in the nanoscale due to the reduction in plasmon phase space, and these particles may be magnetized as well. Hollow interior can further affect such electrochemical properties, while it the structure also enables practical uses as 'inert' containers (e.g., for drug delivery), as well as conduction spheres.[9] The fabrication of different shapes (spheres, cylinders, wires, tubes) has already produced new materials with groundbreaking properties, for example carbon nanotubes, nanocomposites, buckyballs, and graphene. In terms of applications, countless possibilities remain yet to be explored, while nanomaterials are already improving life in countless ways. Due to the many unique properties of nanomaterials, a general catalog of their more major uses, as available online (http://www.understandingnano.com/), can seem to be practically all-inclusive: electronics (transistors), space exploration (carbon nanotube materials), environmentalism and energy (semiconductor NPs in solar cells), food and consumer products (NPs improve fabric quality and kill odors), chemical sensors (carbon nanotubes and ZnO nanowires), and MEMS (lab-on-a-chip devices such as accelerometers). For metal NPs, the literature suggests that commercial ventures have so far mostly dealt in drug delivery.[9, 11]

More particular to gold NPs have been recent and exciting advances in biomedical applications, using their uniquely tunable SPR features. The biocompatibility and facile surface modification of Au material has allowed its colorimetric sensing using its SPR signals to be applied directly to biological cells *in vivo*. This has extended the viability of gold NPs to biomedicine: notably in drug delivery, tissue-tumor imaging, and photothermal therapy.[12] The literature has explored particular applicability of gold NPs for use in cancer treatment.[13, 14] The SPR peaks of gold NPs are tunable to either the visible or IR regions, as desired.[12] These applications all require SPR tuning to the near-IR region, where attenuation by biological elements is at its lowest. According to literature, such tuning cannot be achieved with solidly spherical gold NPs; hence many other methods have been developed: aggregates of spherical particles, nanorods, and composite or hollow spheres.[15] In a related phenomenon, the SPR absorbance can be rapidly converted into heat, as a photothermal effect, which has been effectively applied in combination with drug delivery techniques in order to achieve the targeted destruction of cancer cells.[16] It has also been studied as a useful, controlled variation of conductivity, e.g. via laser annealing.[8] In summary, the desirable characteristics of any AU nanofabrication method will depend on the particular purposes for its products, but many applications all require a primary ability to tune SPR peaks. These peaks are generally dependent on the size, shape, and degree of particle-to-particle coupling, as well as intrinsically on the dielectric properties of the metal (Au) and its substrate (Si). Thus the fabrication method must be characterized primarily by its control of the physical properties of its products – the size, shape, and coupling – as well as by general factors such as its uniformity, its efficiency, its costs, and its scalability. Indeed, many Au nanocage preparations primarily seek to tune the SPR peak to a specifically desired wavelength. Hollow structural interiors can then provide additional opportunity for nanocage modification and their implementation in a wide variety of these as well as potential future applications. Because of the wide number of emerging applications in biomedical fields, coupled with the many available methods of gold NP fabrication, the present future of gold NPs seems to shine bright.

1.3 A brief review of the common method of fabrication for gold nanocages

Facile Au nanocage assembly has been the focus of a wide range of new literature. To date, the most popular methods of metal NP fabrication continue to remain exclusively chemical in nature. The most common traditional preparations of metal NPs have involved the reduction of their salt in solutions (i.e., $HAuCl_4$ for gold (Au), $AgNO_3$ for silver (Ag), $H_2[PdCl_4]$ for Palladium (Pd), and $H_2[PtCl_6]$ for Platinum (Pt)) with a suitable reducing agent (e.g., sodium citrate, borohydride, alcohols, or any of many others).[17] These basic methods of NP production enjoy certain advantages. The entire process remains simple, easy, and cheap, with no need for specialized lab equipment. The product NPs can still be modified by the later addition of suitable agents to tailor the products for specific surface functionalities. Similarly, the simultaneous use of additional reaction agents (or coatings) in the solution can act to help to control the size of the NP product. However, these traditional methods remain constrained by a few basic limitations. Due to the reaction in solution, precise size and shape control remains a great difficulty, and various NPs tend to form simultaneously. Similarly, NPs tend to agglomerate in solution, requiring the use of yet more chemicals to act as stabilizing agents. These effects necessitate purification steps, such as by centrifugation or size-selective precipitation, to filter the product so as to increase NP uniformity. To make any kind of precise product, tight control for reaction times and conditions are required overall.

Many of the newer method of NP fabrication have been developed to achieve particular sizes, shapes, or other properties of the NP products. These advanced techniques can enable specialized applications. A general list of such methods is provided here, with further detail found in the cited research literature: (1) etching[18, 19], (2) electrodeposition[20], (3) galvanic replacement reaction[15], (4) ablation using high peak-power laser pulses[21, 22], (5) direct synthesis onto surfaces[23, 24], (6) synthesis in Langmuir-Blodgett layers[25],

and (7) formation in the gas phase[26, 27]. Overall, these methods represent a wide variety of fabrication approaches, which seem to have little in common other than their result, the Au nanocage products.

A detailed description of one of these advanced methods, the Au / Ag galvanic replacement reaction, presents a good benchmark test for other fabrication methods, in terms of control of the SPR peak.[15, 28] In this procedure, the first step is the preparation of high-quality silver (Ag) nanocubes, which are used as a sacrificial template in the galvanic replacement reaction with gold in the form of $HAuCl_4$. The process requires many carefully controlled steps and takes about 8 hours to complete. The resulting nanocages are precise in that the reaction can be stopped at any time, along a continuous range of the visible color spectrum as displayed by solution. A drawback, besides the sensitivities of the many reaction steps, is that the Au nanocages are impure, because the replacement reaction cannot be allowed to proceed fully to completion, due to the decomposition of the nanocage structure at that stage. Thus, the gold nanocages must contain trace amounts of silver. The products of this procedure are displayed below as a series of colored vials, each containing Au nanocages prepared with the addition of different volumes of 0.1 mM HAuCl4 (aq) solution to the reactant containing dispersed Ag nanocubes (Fig 7).[10] The result of such a preparation, when successful, results in a spectrum of solution colors, each characterized by a uniquely tuned SPR absorbance peak, as indicated below the vials by the displacements between the absorbance peaks. This method has been productively developed in the literature as the basis for a number of further nanoparticle applications and investigations of the potentials of gold nanocages, in various structures (i.e., thin films) and modifications (i.e., annealings) with other interesting ideas.[11, 12]

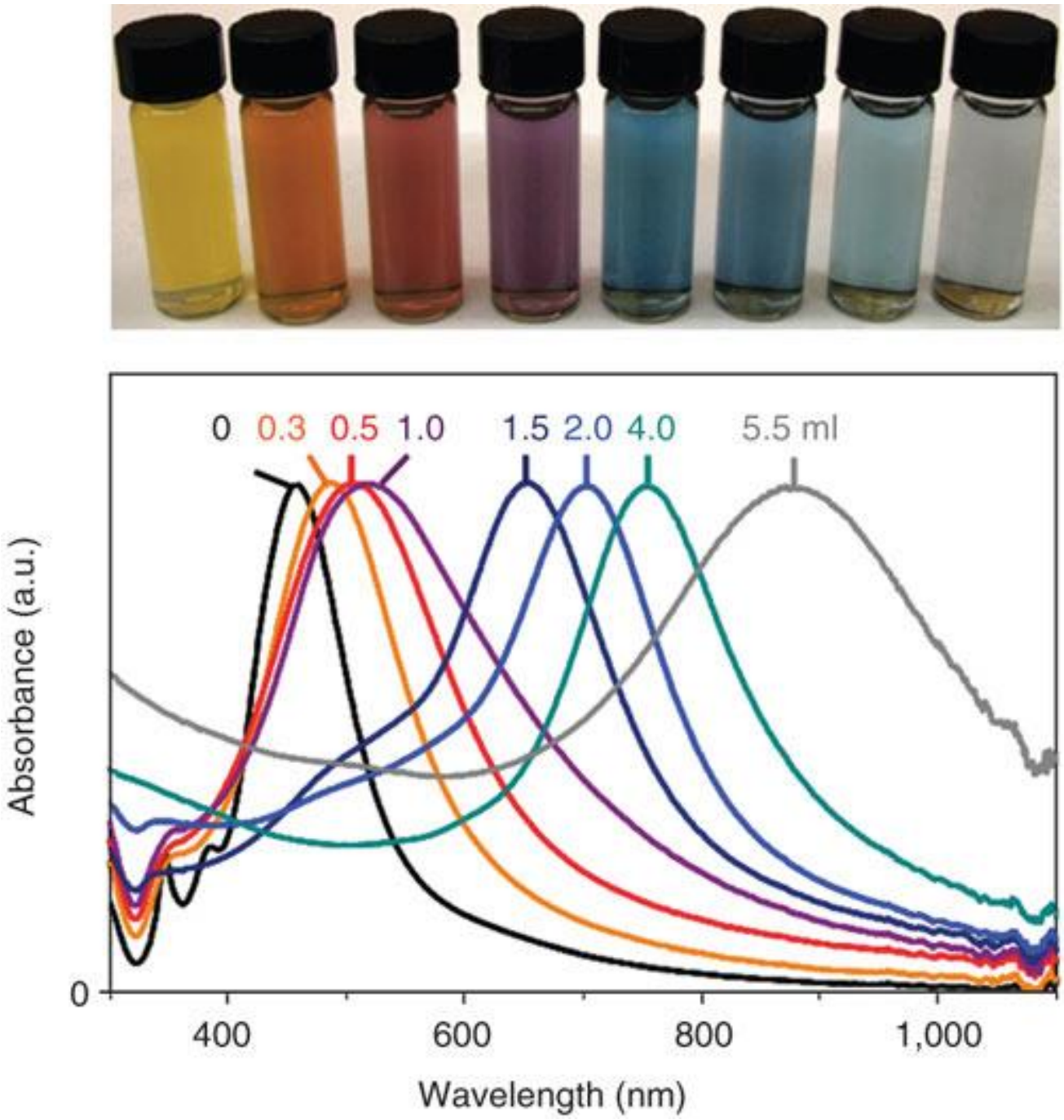

Fig. 7: (Top) Vials containing Au nanocages prepared with the addition of different volumes of 0.1 mM $HAuCl_4$(aq) solution: from left to right, 0, 0.3, 0.5, 1.0, 1.5, 2.0, 4.0 and 5.5 ml, to the reactant containing Ag nanocubes. (Bottom) The corresponding UV-Vis absorbance spectra taken from the Ag nanocubes and Au nanocages. The SPR peak of the Au nanocages is tunable throughout the visible and near-IR regions by varying the volume of $HAuCl_4$ solution added.[10]

1.4 A brief overview of the experimental method of fabrication

The research presented here seeks to characterize a new, easier method of nanocage production with the goal of making the product and its properties just as controllable if not more so than the galvanic replacement reaction and other available alternatives. This method uses photolithography followed by thermal heating as the basis for nanocage production. Few and simple chemical reagents are required for this process fabrication of the gold nanocages: acetone to remove the PMMA resist coat and HF acid to etch the nanocages from silicon. Further, while the heating and cooling process of the furnace step takes several hours, the overall process is generally extremely robust and insensitive to disturbance, unlike many chemical reactions. Finally, an advantage with EBL is that the patterns of gold nanocage products are precisely controllable, as EBL pattern designs can be modified via pattern editing software.

The production steps of this method used Silicon substrate squares of areas on the order of 1 cm x 1 cm. These were cleaned and coated with PMMA, a positive photoresist, using a spin coating method. The PMMA-coated substrates were then used for gold pattern exposures via EBL, which was used to write patterned arrays of areas onto the PMMA coat. The patterns were created using pattern editor software on a separate computer. Once the pattern was written, the gold target was deposited by e-beam evaporation. The PMMA coat was then removed using a simple acetone wash. The patterned gold was then inserted into a high-temperature furnace, where the substrates were heated under fixed heating parameters that resulted in the formation of Au nanocages. The steps of this fabrication process were imaged using SEM and compound light microscopy, to explore its results and its overall useful viability.

This procedure, when fully developed, has good potential to be robust and flexible, as each step can be highly automatized for consistency, and the process involves a large number of controllable parameters. Due to the control of the gold pattern arrangement, precision can be very high for a variety of cases, while procedural uncertainty remains quite low. The method allows a large parameter phase space of fabrication. Specifically, it allows for nanocages to be fabricated from specified parameters for the size of the areas, the area spacings, as well as the depth of the gold deposition per area. The temperature and heating parameters are also expected to influence the shape of the final products, through the thermodynamic conditions in the high-temperature furnace. Finally, because of the simplicity of the thermal heating, this method may be applicable to produce similar products with other types of metal.

The products can be used in a variety of areas including photonics, catalysis, and surface-enhanced Raman spectroscopy-based sensing. The products in this experiment were only imaged using SEM and light microscopy capabilities. For more extensive characterizations and extended applications, it would be advantageous to remove the nanocages from the Si substrates on which they were heated. This was attempted via etching with hydrofluoric acid (HF), but the results were not satisfactory, probably because the amount of gold NPs produced in this experiment was not sufficient to yield samples of colloidal solutions with sufficient NP concentrations, as would be required to perform any TEM analysis.

2.0 Materials and Methods

2.1 Preparation of Clean Silicon Substrates

Silicon substrates were prepared from standard laboratory orders of Si, delivered as circular wafers. The disks were cut into squares using a diamond cutting pen. In the scope of this experiment, the squares were selected to be on the order of 1 cm^2. Different shapes and sizes of the silicon substrates could easily be produced, but the exact size and shape parameters are likely unimportant to the fabrication process. Correspondingly, the substrate shape need not be strictly controlled, neither in straight edges nor in standard geometry. Once cut, the Si squares were then cleaned by submersion in separate solutions of hexanes, ethyl alcohol, and acetone. These steps lasted about 30 seconds and were performed in small beakers under a fume hood. Plastic forceps were used to manipulate the Silicon squares, which were then air dried and stored in a small plastic container. (Metal tools should be avoided, as they may cause damage to the substrate surfaces.) This cleaning was necessary to achieve success in the next step, namely the deposition of the PMMA photoresist coat via spin coating method.

2.2 Addition of a PMMA Coat via Spin Coating

After substrate cleaning, each silicon square was coated with standard laboratory order PMMA 950K. A spin coater uses the centrifugal force of high-speed rotation to spread a coating fluid uniformly over a flat substrate; it makes use of a vacuum pump to secure the substrate during its high-speed rotation, as well as inert N_2 gas flow to decrease the oxygen concentration and to enhance uniformity in the flow mold. Its program parameters were fixed for two steps: a 15 s deposition at 500 rpm rotation speed, during which an amount of PMMA was added via 5 mL plastic syringe, followed by a 45 s rotation at 4000 rpm rotation speed. These parameters were at first varied to investigate differences in deposition.

The primary criterion for success was the amount of PMMA used in the deposition step; less than 2 mL most often resulted in an undesirable non-homogeneous coat, especially for larger substrate areas. To obtain proper coating, an amount of about 2-5 mL of PMMA was required. A deposition step at low rotation speed (500 – 1000 rpm) was needed to apply the entire volume of PMMA, as deposition had to be completed before the start of the high speed rotation to enable uniform spread of the coating. A minimum of 15 seconds for the step seemed to work best. As a rule, higher rotation speed will cause more of the coating liquid to spin off the substrate, so more PMMA is needed to reproduce a desired thickness of coat. The rotation step seemed to achieve best results in the range of 3000 – 4000 rpm for the deposition of 2-5 mL PMMA onto the substrate areas of size 1 cm x 1 cm. Each coated substrate was then immediately heated for 1 minute at 180°C via hot plate, to set the coating. They were stored in a plastic container. When properly coated, the substrates appeared opaque silver-gray in color, while lower amounts of PMMA (i.e., thinner coats) seemed to result in more purple-blue colorings. Anomalies will appear as streaks across the uniform substrate coating, indicating surface contaminants or an uneven flow mold in the spin coater. The spin coater must be wiped down between substrate coatings, as the cleanliness of its mold form results in the aerodynamic features that produce a uniform coating.

2.3 Design of Gold Patterns for the EBL

The gold patterns for the EBL work were designed using the dedicated internal GDSII editor software. The editor has capabilities similar to AutoCAD (such that AutoCAD designs can also be imported for use). For the purposes of this experiment, the arrays were desired to be simple grids of standard geometric shapes (squares and circles), which were expected to yield uniform grid products of gold nanocages. The parameters characterizing the patterns were the shape and size of the individual areas where the gold is deposited (the “Au-areas”) and the spacing between these Au-areas. The Au-areas tested in these experiments ranged in size, with side lengths l = 1 – 80 um for the squares (areas 1 – 6400 um^2), and

circles of corresponding inscribed sizes. Because of the geometric correspondence, this meant that the area of each deposited gold circle was related by the factor π/4 (~80%) to its corresponding circumscribed square area of side length l. The spacing between Au-areas was varied between 1 and 5 um. The Au-areas were arranged in square arrays. For example, a square array of side length 100 um would contain roughly 10 x 10 = 100 Au-areas of square side length l = 8 um each and 1 um spacing separation. Four of such square arrays were arranged together in a grid area of 1 mm x 1 mm, to form a single pattern. Separate patterns were created for various Au-area sizes and various Au-area spacings. The Au-area shape was varied between square and circular, to study the effect of the Au-area shape on the nanocage formation while other parameters are held constant. The pattern orientation was identified by four single geometric shapes written around the origin of the pattern, one for each of the four square arrays. The amount of time a pattern requires for EBL to write its exposure depends on many factors, primarily the pattern size, its complexity (in this case, the number of grid elements), and the exposure parameters set on the EBL system itself (such as the measured beam current). In general, these patterns all required at least 30 minutes for the EBL to complete their exposure; the larger patterns required up to 1 hour each. The time simulation option should be checked in the process of pattern design, to estimate this time. Overall, the exposure of many different patterns can quickly add up to a significant amount of EBL time.

2.4 Gold Patterning via EBL

The EBL patterning was performed with a Raith eLine Lithography system, which functions similarly to an SEM. The samples were inserted via load lock on a sample plate that can carry multiple samples at the same time (5). Before exposure, the e-beam requires general focusing, basic stigmation correction, coordinate field calibration, and write-field alignment. The parameters for exposure were set individually for each case after the automatic step of measuring the beam current, aligning the other

parameters to correspond through adjustment of the dwell time for the three separate cases of line, curve, and dot elements of lithography. The more general parameters that were kept constant for each exposure were the following: magnification of 1000x, focus of 17 mm, and beam voltage of 10 keV. The selection of a coordinate origin point was significant, as this then became the left-hand corner for the field of the Au pattern that was written onto the sample. The origin point was used to write a small generic test pattern, which also included diverse elements to gauge the precision of the lithography for various fundamentals, as well as a way to gauge write field errors using Vernier scales. The time period required to write a desired pattern may be estimated through the 'time simulation' option, but the estimation often seemed to require almost as long as the actual exposure, for patterns of curved elements (i.e., circular Au-areas). In general, a single pattern, a grid of four squares arrays of 100 Au-areas each, required about half an hour to write. For any substrate sample, at least five different patterns were written at a single time, meaning that the whole process took about four hours (half hour focusing, three hour exposure time, and half hour sample insertion and removal). Patterns were written with their addition to a write list, the specification of the coordinates of their left-hand corners, and the selection of layers to expose. Any combination of individual patterns for writing can be automatically performed in a continuous exposure step by adding them to a write list window, specifying their individual coordinates, selecting the layers for exposure, and then using the option 'Write all.' This step cannot be scaled up beyond single substrate, as new coordinate field origins and tilt angle corrections are needed for each substrate. However, a write list may be saved for any combination of patterns, and it can be reused for different substrates, once the substrate coordinate field and tilt angle are redefined.

2.5 Gold Deposition via Electron Beam Evaporation

Once the array patterns have been written onto the PMMA-coated substrate, the gold was deposited by electron beam evaporation. The prepared substrates were inserted on a plate that can carry multiple 1

cm x 1 cm size samples. The rate of gold deposition is controllable, and the progress can be monitored in a real-time sensor display of the depth of gold deposition. Hence, the important parameter of Au-area gold thickness can be controlled. Thickness is significant, as it affects not only the total mass of gold available for nanocage formation, but also the thermodynamic properties of the Au-areas at the high furnace temperatures. For the purposes of this experiment, the thickness was set to be 20 nm. The process of gold deposition requires less than 1 hour, although the evaporator must be equipped with the correct target material, and the cool down phase requires multiple hours before it can be restarted.

2.6 PMMA Mask Removal via Acetone Wash

Once the gold had been deposited and the samples recovered from the evaporator, the PMMA coating had to be removed before proceeding to the last step, nanocage formation by thermal heating. This was accomplished by sample submersion in acetone solution for a period of 1 minute, during which the sample beaker was also exposed to sonification in a water bath. The acetone was seen to remove the PMMA completely. However, first trials also showed that a significant portion of the gold deposition had been damaged by the exposure. The remedy for gold removal by acetone was to use more dilute acetone solution, or even a smaller time frame for the exposure. Ultimately, even with some damage to the Au-areas, around 80% of the total Au-areas were seen to form successful nanocage products. Another interesting observation was that the square Au-areas seemed more susceptible to gold loss than were the circular Au-areas. Finally, the larger Au-areas were clearly more affected by gold loss than smaller ones, so it was easier to use smaller areas (l = 1 um) than larger ones, due to random erosion.

2.7 High-Temperature Furnace Heating

With the removal of the PMMA, the samples were prepared for furnace heating and fabrication of gold nanocage structures. The samples were inserted into a high-temperature furnace with N_2 flow in a glass

rotameter. A handful of samples can be inserted simultaneously. The key parameters of the furnace heating included the following: ramp-up temperature rate, target annealing temperature, time duration of the annealing at constant temperature, and cool-down temperature rate. A further parameter was the N_2 gas flow rate. It was expected that the target annealing temperature could significantly affect the formation of the nanocage structures, in terms primarily of size and perhaps of shape; however, the annealing temperature parameter was not explored during this work. The annealing temperature for this work was set at 938°C, based on the preliminary observations in earlier work that had indicated the formation of promising products for a 10 hr annealing at this temperature, together with constant-rate steps of 5 hr heating and 3.5 hr cooling. Note that while the melting temperature for bulk gold is known to be about 1064°C, the melting point property is well known to vary with size and structure for all NPs, due to their small size and thus their much greater surface to volume ratio.[12, 13, 14] Also, while the theory of NP melting remains unresolved, free NPs are generally theorized to have different (lower) melting temperatures than those supported by a substrate, so that the Si substrate interaction would also affect melting points.[15] The parameters used in this work are shown below in a schematic of the heating step:

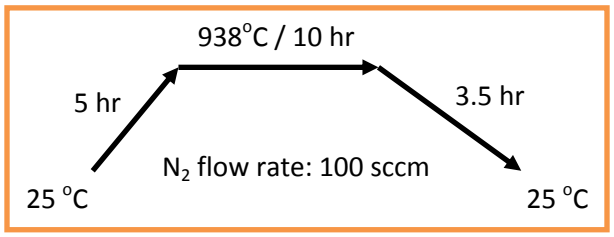

Fig. 8: Parameters for the high-temperature furnace heating; held constant for these experiments

These parameters were all set using the simple programming interface of the high-temperature furnace, which allowed for an automatized procedure that only required manual sample insertion and removal. The thermal heating required 19 hours in total (5 hour heating, 10 hour annealing, and 4 hour cooling). The outcomes of the furnace heating were treated as end products for this fabrication of Au nanocages.

2.8 Isolation of the Gold Nanocages via HF Etching

A further step was explored in the production of gold nanocages, namely that of etching the nanocages off their silicon substrate. This would be desirable because it would allow the formation of gold colloid solutions, which could be easily analyzed by spectroscopic absorbance. These measurements could then be compared to the well-established results of the literature for further validation of this gold nanocage fabrication method. Further, many of the chemical techniques of gold nanocage formation, particularly the commonly cited galvanic replacement reaction, produce gold nanocage colloid solutions as their final product. TEM analysis similarly requires a solution of the gold nanoparticles to use as a sample. Finally, gold colloid solutions are easily transformable into thin film structures that can be characterized by other methods and further exhibit interesting new properties. Thus, etching would be highly desirable for a number of reasons, and it becomes a logical next step for this fabrication procedure. Such an etching was attempted by hydrofluoric acid (HF), which is a strong acid and an extremely hazardous material. Methods of HF etching of similar gold NPs from such Si substrates have been developed and used with success in the literature.[16, 17] The samples were suspended for 30 minutes in a 10% HF solution of DI water. However the etching, while effective in removing some NPs from the sample, did not seem to generate sufficient gold concentration to distinguish the gold nanoparticles under TEM analysis. This indicated that a greater number of nanoparticles would be required for the construction of a gold colloid solution. The samples produced in this experiment were generally not intended for mass fabrication but rather for analysis of parameter effects, so they were not well suitable for use in such an etching process. However, maximum use of the space available for Au pattern lithography on even such a small (1 cm x 1 cm) substrate may be likely to produce enough nanoparticles to allow for effective HF etching. The total substrate area covered by the patterns produced during this experiment was less than one-tenth of the available space. Thus, a larger scale patterning would be a natural extension of this

experimental work, and good test of fabrication viability. The whole etching step takes about 30 minutes. Upon successful etching, a last step would then have to be added to remove the HF from the solution, e.g. using vacuum evaporation, since the boiling point of HF acid is known to be a low 19.5^{o}C. After this was accomplished, the final product would be a gold colloid suspension in water, as desired.

2.9 Imaging by SEM and Compound Light Microscopy

The various stages of the fabrication process were imaged using a simple compound-light microscope as well as the SEM capabilities of the EBL machine. The following three stages of fabrication were imaged: after EBL pattern lithography (step 4), after PMMA removal (step 6), and after furnace heating (step 7). The use of e-beam imaging would damage the photosensitive PMMA coating; so the first of these three stages must be performed by simple compound light microscopy. The second stage was similarly imaged on the compound light microscope, to enable better comparison of the first and second stages. The third stage was imaged by the SEM microscopy of the EBL machine, with enough resolution to identify the three-dimensional structural features of the products. While an SEM is not well-equipped to show three-dimensional structure, the literature has suggested differential tilt imaging as a way to capture certain three-dimensional features. Unfortunately, this was not possible on the EBL machine, because it did not have the capability to tilt samples. Nevertheless, a spherical nanocage structure was strongly indicated by the circular shape of the product, along with the contoured shape as revealed through different focus lengths. An important property that not revealed by the SEM images was whether the nanocages exhibited hollow structural features. As the SEM did not penetrate past the gold surfaces, TEM microscopy would be required to achieve greater resolution. Hence, the analysis of more detailed structural features of the nanocages requires their production to a concentration that allows the etching (step 8), which would enable the TEM analysis that would yield a more detailed optical characterization.

3.0 Results and Discussion

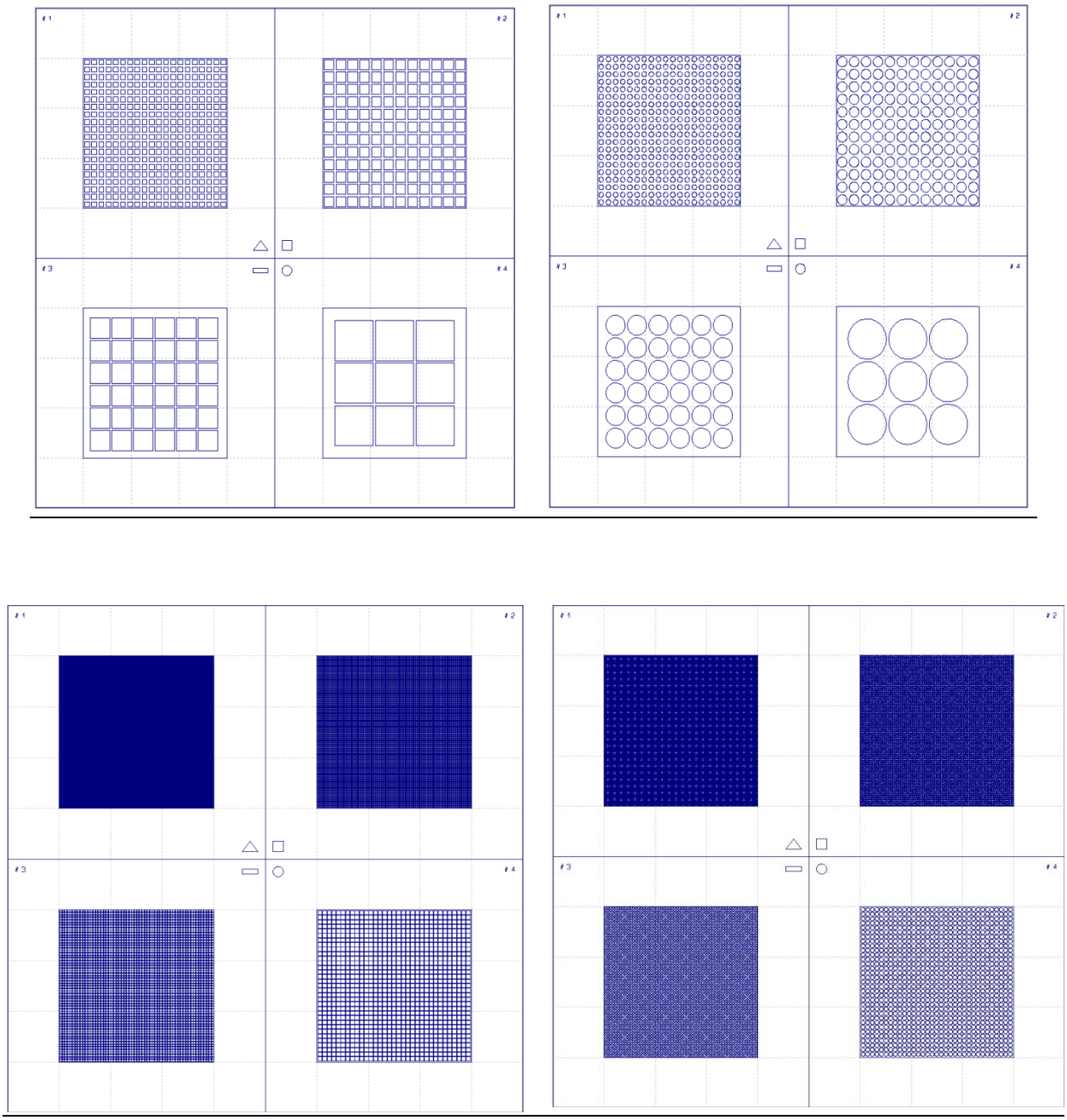

Fig. 9: Representative pattern constructions from images taken in the pattern editor, for both square and circular Au-areas of edges (a) l = {10 um, 20 um, 40 um, 80 um} and (b) l = {1 um, 2 um, 4 um, 8 um}.

The patterns used for the EBL exposure were created using pattern editor software, with capabilities similar to any design program, as well as the additional feature to add layered designs for EBL exposure. The general pattern design comprised a large grid array composed of four smaller squares, arranged around a central orientation pattern of distinct geometric structure to mark each of the four quadrants (a triangle, square, rectangle, circle, respectively) (Fig. 9). Some patterns were created with different size areas in the quadrants, for purposes of comparison, and others were created with uniform size areas in the quadrants, for purposes of product uniformity. The representative patterns featured here were used to indicate that an entire range of desired size areas may be efficiently explored with only a few pattern designs, say four (i.e., l = 1 – 10 um, 10 – 100 um, 1 – 50 nm, and 100 – 500 nm), which can all be written on a single substrate. This allows different heating parameters to be explored using a constant sample template of different size areas, to investigate the effects of their formation. The pattern shapes were produced for both circular and square shapes, to highlight the shape of the area as a controllable parameter, even though the results indicated that this did not result in any effect on the final product. All of the patterns produced in this way were added to the same pattern layer, so that the entire pattern was exposed simultaneously, but this can be modified to allow for more versatility in any pattern design.

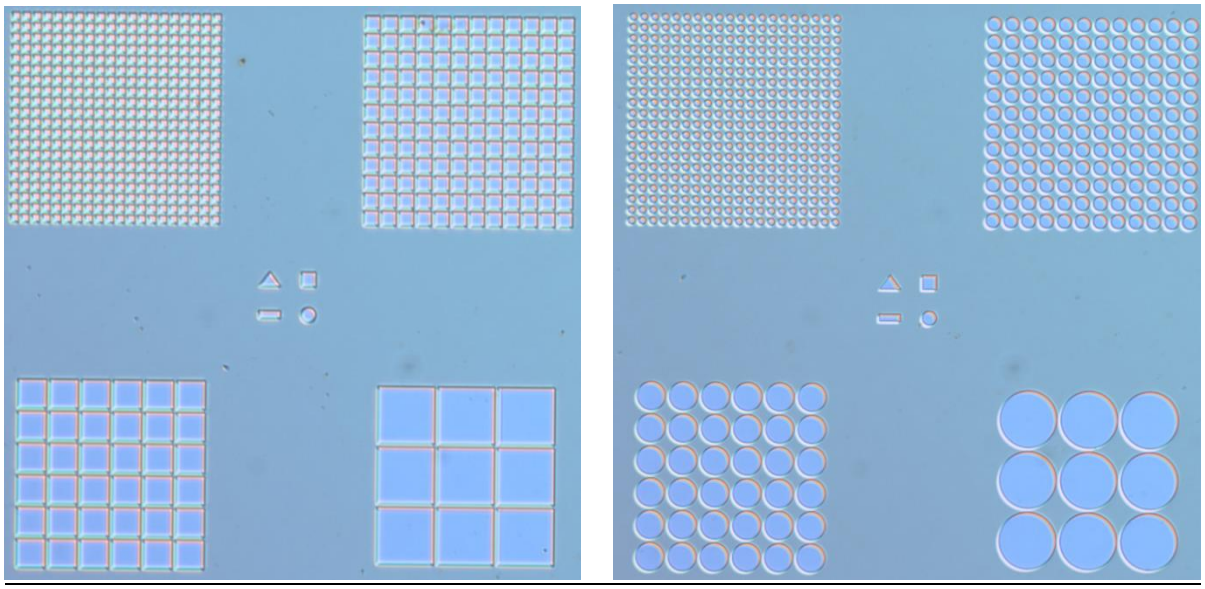

Fig. 10: Light microscopy images of entire single patterns, for equivalent size (a) squares and (b) circles.

Written patterns were imaged in entirety to verify their consistent production with no error or defect (Fig. 10). At this stage, before gold deposition, the patterns were only indentations in the thin PMMA coating. Many types of patterns similar to these were written onto every sample, in different positions.

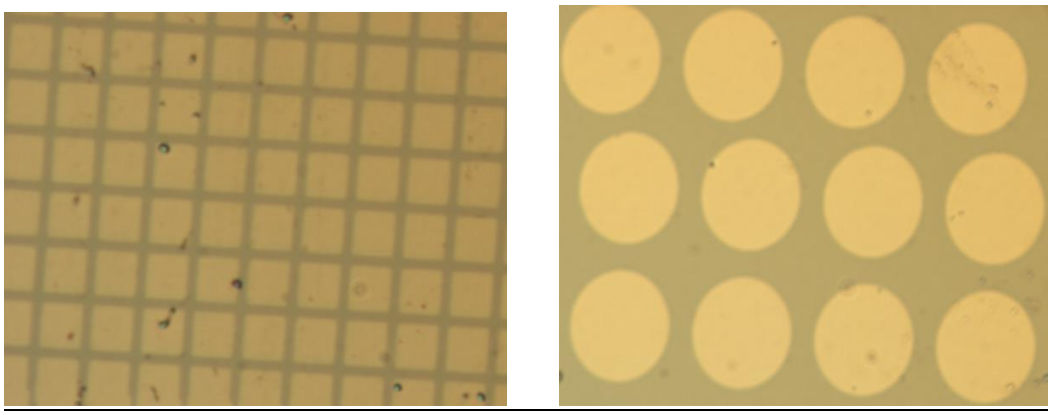

Fig. 11: Light microscopy of EBL patterns revealed high success using both (a) squares and (b) circles.

The precision of the EBL exposure resulted in consistently high success of exposure pattern uniformity, for patterns designs of various shapes, spacings, and sizes (Fig. 11). These images were compared to their complements at later stages of the fabrication process, to investigate problems with the process.

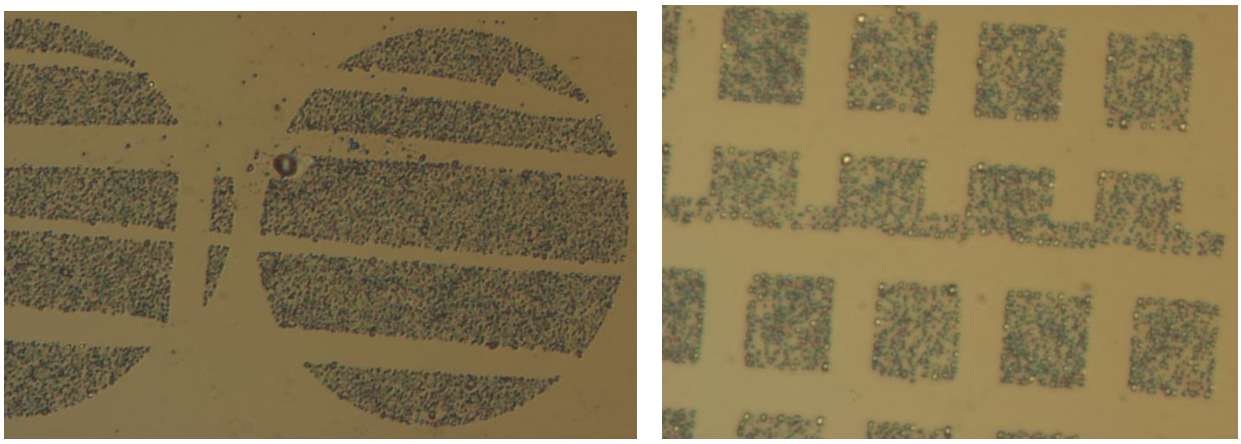

Fig. 12: Light microscopy highlights the two major sources of error: (a) the loss of gold area during the PMMA coat removal by acetone, and (b) the distortion of pattern area due to write field alignment error

The experimental results revealed two steps in the fabrication procedure that require close control: the handling of the sample exposure in the acetone wash and the EBL manual write field alignment (Fig. 12).

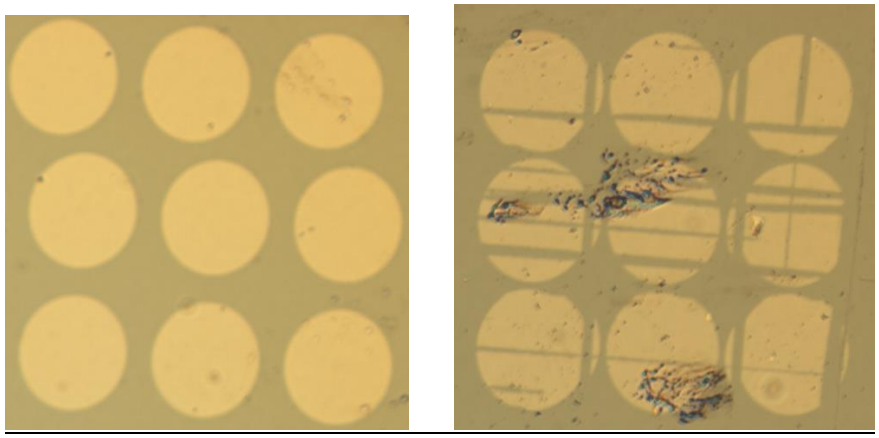

Fig. 13: Light microscopy revealed the effects of poor write field alignment during EBL in (b) vs. (a). These error effects seemed to cause more gold loss to acetone exposure during removal of the PMMA.

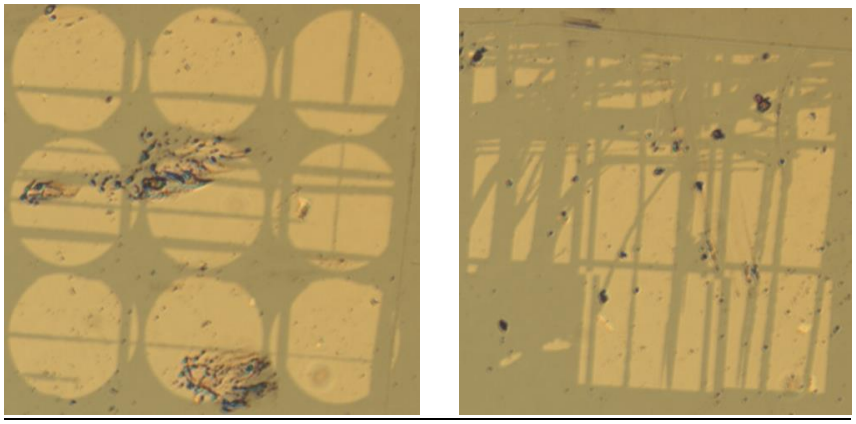

Fig. 14: Light microscopy after acetone wash revealed less gold loss for (a) circles than for (b) squares.

The loss of gold area to the acetone wash was the result of the need to remove the PMMA resist coat before the thermal heating step. While PMMA should etch much more easily and quickly in acetone, it seemed that a small fraction of the gold area was also etched away during the 1 minute exposure with

sonification. The gold loss seemed to be most exacerbated in areas already fragmented by write field alignment error, which seems to provide the primary motivation for careful elimination of that previous problem (Fig. 13). This error was most commonly visible in thin streaks across the gold areas, with some areas affected more than others. In general, it seemed that square areas were more susceptible to damage than were the circular areas (Fig. 14). This small observation was, in fact, the only difference between circular and square patterns noted in the experimental procedure. In any case, a large majority of the gold (over 80%) was recovered intact in even the worst of trials. The solution to this problem was a shorter exposure time to acetone, with less sonification. The PMMA seemed to fall off rapidly in the first few seconds of exposure, so this step should be shortened to achieve a higher final product yield.

The error of the write field alignment is derived from the EBL pattern writing, depending on the quality and precision of the alignment focus manually obtained on the EBL machine prior to exposure. The EBL exposure proceeded through steps of l = 100 um size square 'write fields' of the pattern design, between which the EBL system physically moves the sample stage to continue the exposure. For poor manual write field alignments, the borders of the write fields fail to match well, creating a noticeable edge effect in any section of the pattern along a write field boundary. The solution to this problem was simply to ensure highly precise alignment prior to exposure. Alternatively, the entire pattern may also be written to avoid splitting across the write field boundary. Thus, the smaller size areas were in this consideration easier to write than the larger ones, as they did not intersect the write field boundaries, while the larger ones inevitably did. However, even when this error was most noticeably present, its effect did not seem to detract from the final results, as areas of large size were intrinsically fragmented by the heating process in any case, regardless of the unintended separation due to the write field error.

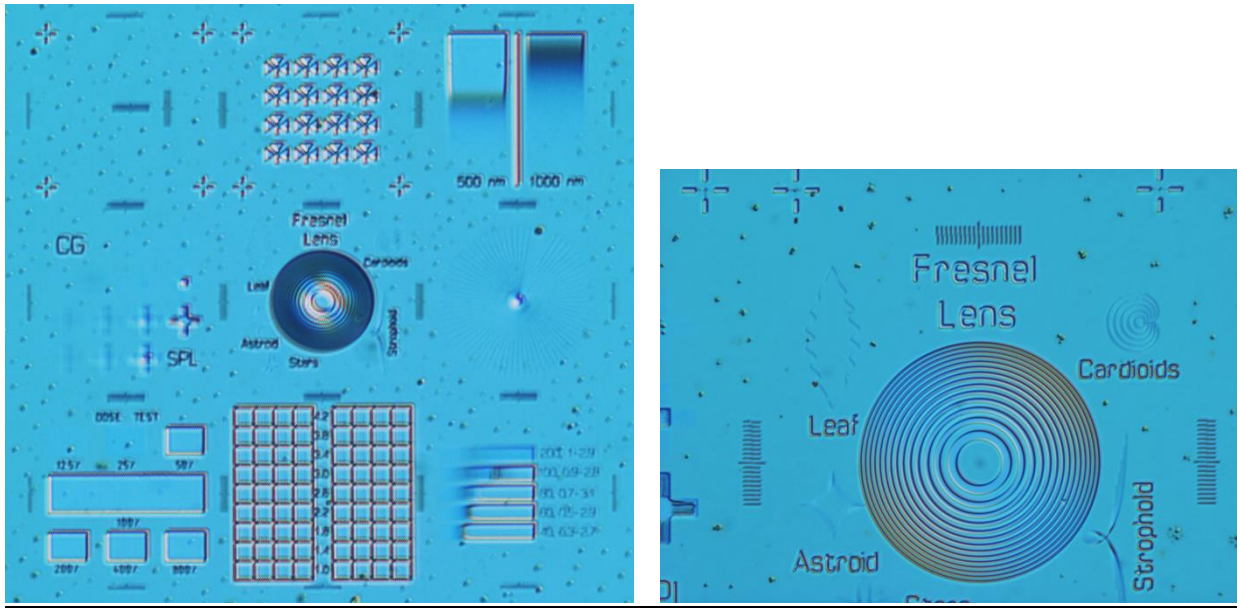

Fig. 15: Light microscopy images of (a) entire test pattern with its various elements, and (b) a highlight of its Vernier scales (above and to either side of the spheroid), used as a gauge of write field alignment.

The general conditions of the pattern condition for each EBL exposure on a substrate was recorded with a generic test pattern, included on every substrate (Fig. 15). Among its many lithographic elements, most of which serve to test the precision of lithographic capabilities for the given conditions of focus and alignment, the most relevant for these patterns were the Vernier scales above and to either side of the central spheroid. These measure the write field alignment, as they are positioned at the write field boundary. A mismatch of the Vernier scale origins indicated the degree of write field error; similarly, the accurate alignment of the Vernier scale origins indicates very low write field error. As in the featured image, these origins were well aligned in almost every case, due to manual efforts for good alignment. The test pattern was significantly smaller than the gold patterns, and it was always written first in the coordinate origin (0, 0) position as defined on the substrate. It experienced uniform gold deposition as part of the surface, and its pronounced gold loss during the acetone wash supported the idea that small, fragmented gold areas were more susceptible to removal by acetone than were solid, coherent areas.

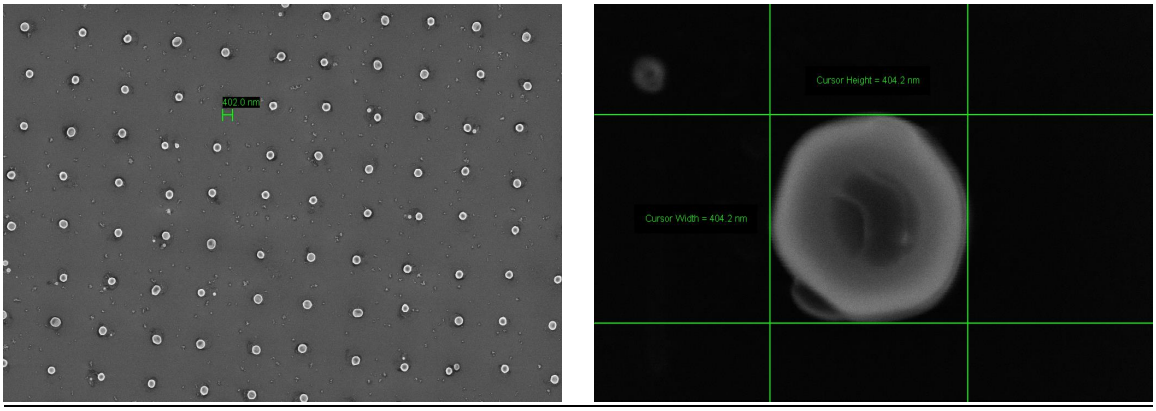

Fig. 16: SEM images of l = 1 um areas revealed (a) grid arrays (5K x) of (b) singular nanocages (100K x).

As mentioned in the introduction, the nanocage products formed by high-temperature furnace heating were not removed from the substrate via HF etching, due to low levels of total nanocage concentration. So the entirety of the characterization and analysis steps were performed via light microscopy and SEM. This analysis revealed that the thermal fabrication – with the parameters described earlier – consistently and uniformly produced nanocage structures on the order of 400 nm in diameter from the 1 um^2 size Au-areas (Fig. 16). The grid array of the pattern was well discernable in the arrangement of these final products. The spherical shape of the products was naturally suggested as a thermodynamically favorable structure. This conclusion was supported by SEM analysis, but the 3D structure was not well revealed.

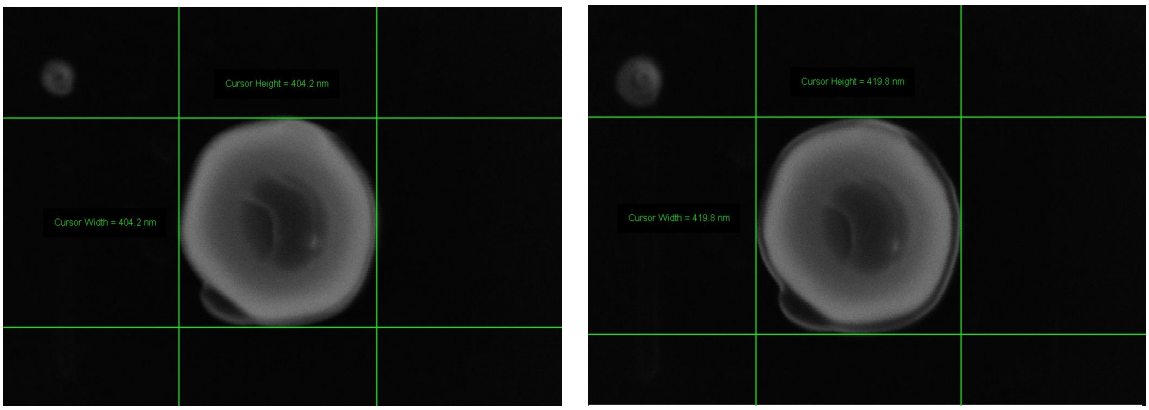

Fig. 17: SEM images of l = 1 um areas revealed nanocage uniformity for both (a) circles and (b) squares.

All of the individual gold nanocages displayed uniform, circular contours (Fig. 17). The uniform gold nanospheres of ~400 nm diameter were all produced from Au mass deposits of dimension 1 um^2 area by 20 nm thickness, for a total gold volume of 1.99E+07 nm^3 per Au-area. For the assumption of spherical NP shape, the radius as obtained from the SEM analysis of an individual product (e.g., 212 nm in Fig. 17(b)) can be related to the earlier discussion of the properties of solid gold nanospheres (Table 1). A solid gold nanosphere of radius 212 nm would have a volume of 3.99E+07 nm^3 or 2 um^2 x 20 nm, which would be twice the available gold mass on the sample. Complementarily, an Au-area volume of 1.99E+07 nm^3 could form a solid gold nanosphere of maximum radius 168 nm, which would be far less than the value obtained from the image. Consequently, measurements from the SEM images yielded the observation that the volume of the product nanospheres was more than equal to the volume of the gold deposit available for NP formation. This conclusion suggested that these nanocage products must be roughly half hollow in their interior structure. The SEM analysis did not have the capability to probe the finer atomic structure of the nanocage products, nor was it sufficient to resolve internal structure. These considerations and features of hollowness may be resolvable by the higher resolutions of TEM analysis.

Literature has indicated that plasmonic effects and the associated SPR property, which of all the gold NP characteristics may be the most desirable to tune, start to attenuate at roughly 150 nm size diameters (see Fig. 2). Thus these products, despite their uniformity and very likely hollowness in large part, would nevertheless be too large to exhibit SPR effects, should they be converted to a form of colloid solution.

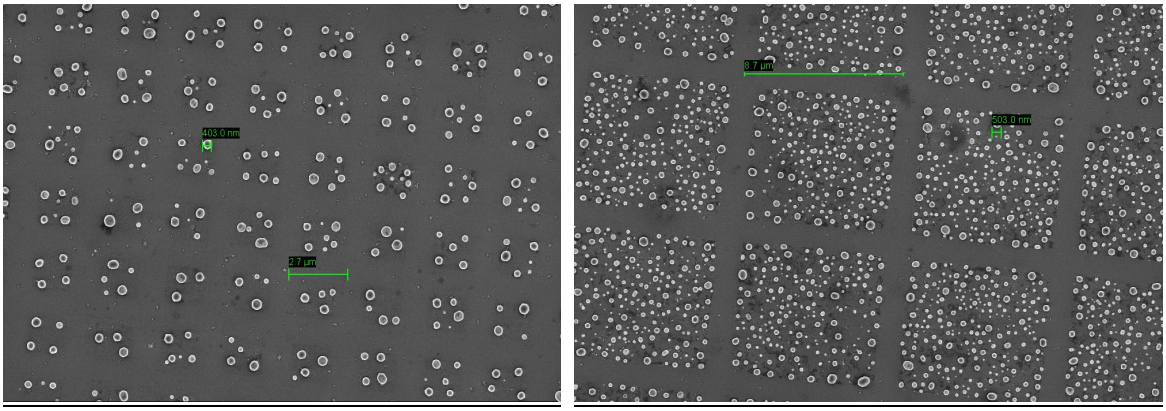

Fig. 18: SEM images of larger (a) l = 2 um and (b) l = 8 um areas revealed area fragmentation of products.

The larger areas (from l = 2 um up) were revealed under SEM to fragment into products of comparable size to the single products made of the l = 1 um areas (Fig. 18). Specifically, the l = 2 um size areas were seen to fragment rather uniformly into about four (up to six) individual products, with a greater range in their sizes but the same average size as before (~400 nm diameter). This suggested a relatively strong relation between the area size and the total number of fragmented products, indicating that the thermodynamic conditions at these parameters favored the formation of gold nanocages at a specific size diameter. The l = 8 um size areas reinforced this trend, with a proportionally greater number of fragmented products, as well as a similarly greater size range between the individual products. Another discernable trend was that the randomness of the product arrangements increased rapidly with the greater fragmentation of the area, with the products more haphazardly spaced throughout any single l = 8 um size area. This increase in the randomness of distribution was accompanied by a relative increase in the number of smaller structures, as opposed to average size structures. The trend toward randomness continued with larger size areas, so these results indicated that the products would form with uniformity for a maximum size of l = 1 um, for these conditions. In fact, the largest areas showed poor structural forms in general, with significantly more degeneration of structural shapes and the prevalence of smaller, 'flatter' objects.

The amount of spacing between the areas was not seen to affect the formation of products in any case, as neighboring areas did not seem to exhibit any interaction at all during the thermal heating. In effect, this allowed the area spacing to be reduced to a minimum, which is desirable for a number of reasons, including higher product saturation level per area substrate, faster EBL write times due to the smaller write areas, and more compact pattern designs along with achievable nanocage arrangements. Finally, the products and overall results were equivalent, regardless of whether the gold areas had been square or circular in geometric shape, given comparisons of the same size areas (Fig. 17). This meant that the total mass of gold available for the formation by thermal heating was much more significant than the shape of the area, which seemed to have no effect at all. Overall, this finding should seem unsurprising, as the difference between area geometries represents only small edge effects, while the larger effects of thermodynamic heating, gold thickness, and amount of gold area all remain the same across both cases. The complementary compound light microscopy reinforced the conclusions gained from SEM imaging.

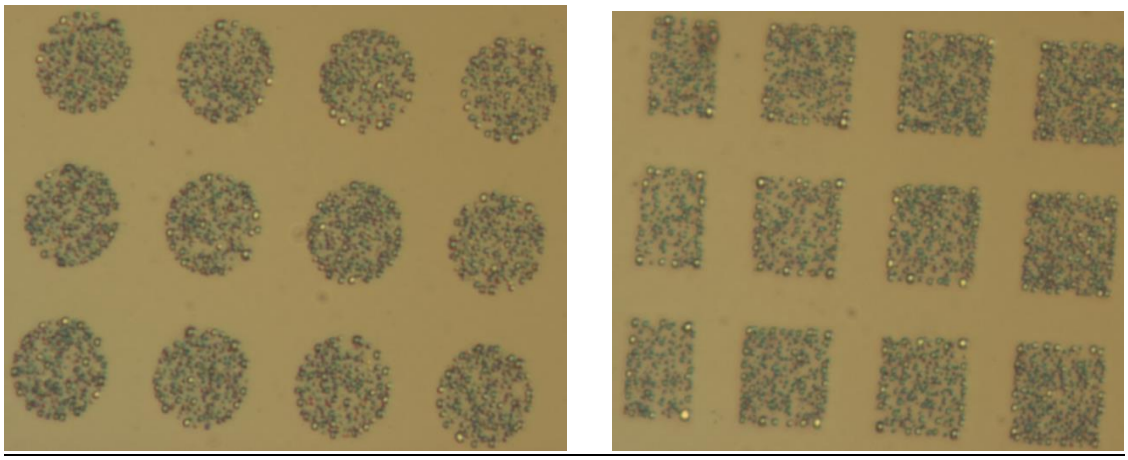

Fig. 19: Light microscopy confirmed consistent area fragmentations in both (a) circles and (b) squares.

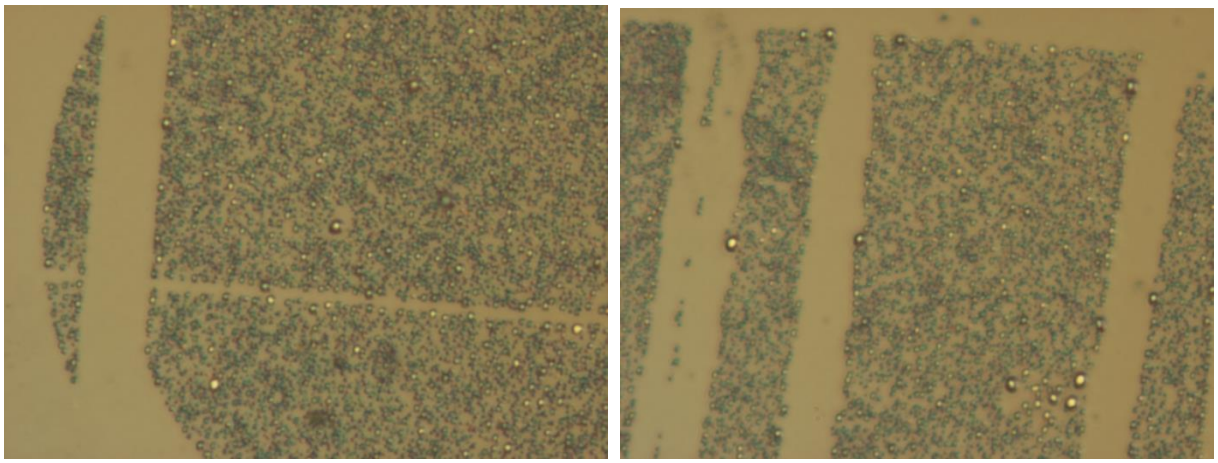

Fig. 20: Light microscopy revealed larger areas (l = 80 um featured here) caused increasingly inconsistent and non-uniform product formation in both (a) circular patterns and (b) square patterns.

The increasing fragmentation of larger areas was confirmed for both circle and square patterns (Figs. 19-20). As an uncontrollable, random effect of the fabrication process, such area fragmentation was treated as an undesirable feature. It can be mitigated by restriction of the pattern designs to smaller Au-areas.

4.0 Conclusion

The results collected so far did not provide sufficient evidence to determine whether or to what extent this thermal fabrication method may allow for the facile fabrication of various versatile gold nanocages. Time constraints and a steep learning curve prevented the complete characterization of the procedure, and the most interesting analysis – investigation of the plasmonic characteristics of the gold nanocage products – remains unfortunately unrealized. Nevertheless, insight regarding the fabrication method and its viability was obtained from these results, a summary of which may prove valuable in future work.

The project demonstrated that the thermal fabrication method for gold nanoparticles could use silicon substrates repeatedly to produce large, uniform gold nanospheres of about 400 nm in diameter from Au deposits of 1 um^2 areas and 20 nm thicknesses. SEM images showed the volume of such nanospheres to be greater than the volume of the gold deposit available for nanoparticle formation, which suggested that the nanocage products were hollow, at least in part. Larger gold deposits (> 1 um^2) were all characterized by area fragmentation into multiple nanoparticles, undesirable due to the much greater variation in their size. The best product uniformity was achieved in the case where each Au-area formed a single nanocage; thus, the isolated spacing of properly sized Au-areas would seem to be a condition for the fabrication of a uniform product. As long as this intrinsic limitation cannot be circumvented or the EBL exposure step improved in time efficiency, the thermal fabrication method may be rate-limited to the production of relatively small numbers of nanoparticle products, in quantities not easily convertible to nanoparticle suspensions. As the spacing separation size between Au-areas did not affect product formation, spacing may be minimized. The research results suggested the best way to produce uniform gold nanocage products with this method would be to reduce the size of the Au-area deposits and to

minimize their separation, increasing the product yield. Since NP uniformity with no area fragmentation was achieved for NPs of 400 nm diameter, smaller size NPs can be anticipated to form uniformly as well.

Specific observations that were made at each fabrication step may also prove useful for the future work:

(1) The PMMA spin coating was most reliably successful when 2-5 mL of PMMA was used for a sample substrate of size order 1 cm x 1 cm, with a 45s rotation step in the range 3000-4000 rpm.

(2) The precision of the write field alignment entailed greater errors for larger Au-areas than for smaller ones. It should diminish in importance for the smaller Au-areas of future experiments.

(3) The shape of the Au-deposits (e.g., circles vs. squares) and the spacing between them were not significant parameters in the determination of the final product. The spacing may be minimized.

(4) The exposure of the sample to the acetone wash should be kept short (< 1 min.) with a small amount of sonification, in order to minimize the loss of gold area during the PMMA removal.

5.0 Acknowledgements

This work was completed with the Professor James Dickerson research group and its facilities at Vanderbilt University. The work mostly used the facilities of the Vanderbilt Institute for Nanoscale Science (VINSE), specifically: the Electron Optics Laboratory (Raith EBL machine, the SEM and TEM machines, and the PMMA Spin Coater), the Nanocrystal Fabrication Laboratory (the Pattern Editor computer), the Nano-Carbon Laboratory (the e-beam Evaporator), and the High-Temperature Furnace. Special thanks are due to Dr. Anthony Hmelo, as VINSE laboratory director; Dr. Bo Choi, for valuable assistance with the use of the e-beam Evaporator; and Weidong He, for great help as a graduate student mentor as well as for his active participation in the progress and development of this research project.

References

(1) Mie. **Beiträge zur Optik trüber Medien, speziell kolloidaler Metallösungen**. *Annalen der Physik*, Vierte Folge, Band **25**, No. 3, pp. 377-445 (1908). Translated to English for Sandia Labs, July 1978: "**Contributions on the Optics of Turbid Media, Particularly Colloidal Metal Solutions."** Available Online via http://www.scattport.org/index.php/gustav-mie-special.

(2) Tcherniak, Ha, Domingues-Medina, Slaughter, and Link. **Probing a Century Old Prediction One Plasmonic Particle at a Time**. *Nano Letters*, Vol. 10, pp. 1398-1404 (2010). doi:10.1021/nl100199h.

(3) Khlebtsov. **Optics and Biophotonics of Nanoparticles with a Plasmon Resonance**. *Quantum Electronics*, Vol. 38, Issue 6, pp. 504-529 (2008). doi:10.1070/QE2008v038n06ABEH013829.

(4) Stoleru and Toew. **Optical Properties of Nanometer-Sized Gold Spheres and Rods Embedded in Anodic Alumina Matrices**. *Applied Physics Letters*, Vol. 85, No. 22, 5152-5154 (2004). doi:10.1063/1.1828233.

(5) Kreibig and Vollmer. **Optical Properties of Metal Clusters (Springer Series in Material Science).** Springer: New York, 1995.

(6) Skrabalak, Chen, Sun, Lu, Au, Cobley and Xia. **Gold Nanocages: Synthesis, Properties, and Applications**. Acc. Chem. Res. 2008 December; 41(12): 1587-1595. doi:10.1021/ar800018v.

(7) Chen, Wang, Xi, Au, Siekkinen, Warsen, Li, Zhang, Xia, and Li. **Immuno Gold Nanocages with Tailored Optical Properties for Targeted Photothermal Destruction of Cancer Cells**. *Nano Letters*, Vol. 7, pp. 1318-1322 (May 2007). doi:10.1021/nl070345g.

(8) Cheng, Uang, Wang, Chiou and Lee. **Laser Annealing of Gold Nanoparticles Thin Film using Photothermal Effect.** *Microelectric Engineering*, Vol. 86, Issues 4-6, p. 865-867 (April-June 2009). doi:10.1016/j.mee.2008.12.058.

(9) Bohren and Huffman. **Absorption and Scattering of Light by Small Particles.** Wiley, Inc.: New York, 1983.

(10) Feynman. **There's Plenty of Room at the Bottom**. *Science* Vol. 254, pp. 1300 – 1301 (1991).

(11) Salata. **Applications of Nanoparticles in Biology and Medicine.** *Journal of Nanobiotechnology*, Vol. 2, Issue 3 (2004). doi:10.1186/1477-3155-2-3.

(12) Skrabalak, Chen, Au, and Lu, Li, and Xia. **Gold Nanocages for Biomedical Applications.** *Advanced Materials*, Vol. 19, Issue 20, pp. 3177-3184 (2007). doi:10.1002/adma.200701972.

(13) Skrabalak, Au, Lu, Li, and Xia. **Gold Nanocages for Cancer Detection and Treatment.** *Nanomedicine*, Vol. 2, No. 5, pp. 657-668 (2007). doi:10.2217/17435889.2.5.657.

(14) Cai, Gao, Hong, and Sun. **Applications of Gold Nanoparticles in Cancer Nanotechnology.** *Nanotechnology, Science and Applications*, Vol. 1, pp. 17-32 (2008). doi:10.2147/NSA.S3788**.**

(15) Skrabalak, Au, Li, and Xia. **Facile Synthesis of Ag Nanocubes and Au Nanocages**. *Nature Protocols,* Vol. 2, pp. 2182 - 2190 (2007). doi:10.1038/nprot.2007.326.

(16) Cobley, Au, Chen, and Xia. **Targeting Gold Nanocages to Cancer Cells for Photothermal Destruction and Drug Delivery.** *Expert Opinion on Drug Delivery*, Vol. 7, No. 5, pp. 577-587 (2010). doi:10.1517/17425240903571614.

(17) Kurniawan, Fredy. **New Analytical Applications of Gold Nanoparticles**. Ph.D. Dissertation, submitted to the University of Regensburg, Germany in February 2008. Published online in 2009. Available online http://epub.uni-regensburg.de/12113/1/Fredy_Kurniawan_desertation.pdf.

(18) Jensen, T. R.; Schatz, G. C.; Van Duyne, R. P. **Nanosphere Lithography: Surface Plasmon Resonance Spectrum of a Periodic Array of Silver Nanoparticles by Ultraviolet-Visible Extinction Spectroscopy and Electrodynamic Modeling.** *J. Phys. Chem. B*, Vol. 103, No. 13, pp. 2394-2401 (1999).

(19) Hulteen, J. C.; Treichel, D. A.; Smith, M. T.; Duval, M. L.; Jensen, T. R.; Van Duyne, R. P. **Nanosphere Lithography: Size-Tunable Silver Nanoparticle and Surface Cluster Arrays.** *J. Phys. Chem. B*, Vol. 103*,* No. 19, pp. 3854-3863 **(**1999).

(20)Kim, S. S.; Nah, Y. C.; Noh, Y. Y.; Jo, J.; Kim, D. Y. **Electrodeposited Pt for Cost-Efficient and Flexible Dye-Sensitized Solar Cells.** *Electrochimica Acta,* Vol. 51, No. 18, pp. 3814-3819 (2008).

(21)Ullmann, Friedlander, Schmidt-Ott. **Nanoparticle Formation by Laser Ablation**. *Journal of Nanoparticle Research*, Vol. 4, No. 6, pp. 499-509 (2002).

(22)Simakin, Voronov, Kirichenko, Shafeev. **Nanoparticles Produced by Laser Ablation of Solids in Liquid Environment**. *Applied Physics A: Materials Science & Processing*, Vol. 79, No. 4, pp. 1127-1132 (2004).

(23)Reetz, Winter, Dumpich, Lohau, and Friedrichowski. **Fabrication of Metallic and Bimetallic Nanostructures by Electron Beam Induced Metallization of Surfactant Stabilized Pd and Pd/Pt Clusters.** *J. Am. Chem. Soc.*, Vol. 119, No. 19, pp. 4539-4540 (1997).

(24)Saurakhiya, Zhu, Cheong, Ong, Wee, Lin, and Sow. **Pulsed Laser Deposition-Assisted Patterning of Aligned Carbon Nanotubes Modified by Focused Laser Beam for Efficient Field Emission.** *Carbon*, Vol. 43, No. 10, pp. 2128-2133 (2005).

(25)Moriguchi, Shibata, Teraoka, and Kagawa. **Control of Size of CdS Formed in Organized Molecular Assembly Films by Molecular Structure and Film Orderliness.** *Chemistry Letters*, Vol. 24, No. 9, pp. 761-762 (1995).

(26)Kruis, Fissan, and Peled. **Synthesis of Nanoparticles in the Gas Phase for Electronic, Optical and Magnetic Applications -- a Review**. *Journal of Aerosol* Science, Vol. 29, Nos. 5-6, pp. 511-535 (1998).

(27)Hahn. **Gas Phase Synthesis of Nanocrystalline Materials.** *Nanostructured Materials*, Vol. 9, Nos. 1-8, pp. 3-12 (1997).

(28) Lu, Chen, Skrabalak, and Xia. **Galvanic Replacement Reaction: A Simple and Powerful Route to Hollow and Porous Metal Nanostructures.** *Proceedings of the Institution of Mechanical Engineers, Part N: Journal of Nanoengineering and Nanosystems*, Vol. 221, No. 1, pp. 1-16 (2007). doi:10.1243/17403499JNN111.

(29) Muller, Mornaghini, and Spolenak. **Ordered Arrays of Faceted Gold Nanoparticles Obtained by Dewetting and Nanosphere Lithography.** *Nanotechnology*, Vol. 19, No. 48, (2008). doi:10.1088/0957-4484/19/48/485306.

(30) Kuiri, Lenka, Ghatak, Sahu, Joseph, and Mahapatra. **Formation and Growth of SnO_2 Nanoparticles in Silica Glass by Sn Implantation and Annealing.** *Journal of Applied Physics*, Vol. 102, Issue 2 (2007). doi:10.1063/1.2761778.

(31) Koga, Ikeshoji, and Sugawara. **Size- and Temperature-Dependent Structural Transitions in Gold Nanoparticles.** *Physics Review Letters*, Vol. 92, Issue 11 (2004). doi:10.1103/PhysRevLett.92.115507.

(32) Buffat and Borel. **Size Effect on the Melting Temperature of Gold Particles.** *Physics Review A*, Vol. 13, Issue 6, 2287–2298 (1976). doi:10.1103/PhysRevA.13.2287.

(33) Farrell and Van Siclen. **Binding Energy, Vapor Pressure, and Melting Point of Semiconductor Nanoparticles.** *Journal of Vacuum and Science Technology B*, Vol. 25, pp. 1441 - 1448 (2007). doi:10.1116/1.2748415.

(34) Jiang et al. **Theoretical Study of the Thermal Behavior of Free and Alumina-Supported Fe-C Nanoparticles.** *Phys. Rev. B,* Vol. 75 (2007). doi:10.1103/PhysRevB.75.205426.

(35) Hessel, Heitsch, and Korgel. **Gold Seed Removal from the Tips of Silicon Nanorods.** *Nano Letters*, Vol. 10, pp. 176–180 (2010). doi:10.1021/nl903235e.

(36) Chapple-Sokol et al. **Safe Method for Etching Silicon Dioxide**. U.S. Patent 5,268,069, filed June 8, 1992 and issued Dec. 7, 1993. Available online http://www.patents.com/us-5268069.html.

Original Project Proposal:

This yearlong Independent Research project will pursue a new, simpler method of gold nanocage production that uses thermal and surface chemical techniques, not solution-phase chemistry. The experimental nature of the project is emphasized, as the student will learn and then refine the algorithms that lead to the fabrication of the nanomaterials. This project will involve use of the photolithographic facilities of the Vanderbilt Institute of Nanoscale Science and Engineering (VINSE) to produce arrays of gold nanoparticles, deposited onto silicon sheets, from which the gold nanocages will be synthesized. The production process will also employ high-temperature furnace facilities, supplied by the Dickerson Group, to induce surface energy-driven reformation of the nanoparticles, varied as functions of time and temperature. The resultant structures will be analyzed using transmission electron microscopes and scanning electron microscopes provided by VINSE. The primary goal of the project is to perform a battery of experiments to ascertain the phase space of parameters that are involved in the nanocage production: specifically, the set point temperature, the thermal ramping time, the set point dwell time, the gold film thickness, and the gold nanoparticle initial diameter. Upon ascertaining the optimum conditions within this parametric space, the physical characteristics of the gold nanocage arrays and nanocages can be explored, particularly the plasmonic response or the electrical conductivity.

The primary work days will be Monday, Wednesday, Friday, and the weekend, with respective target work hours of 11 AM – 6 PM, 10 PM – 1 PM, 12 PM – 6 PM, and 2 PM – 6 PM, respectively. Lunch meetings with the Dickerson group will occur once a week, between 10 AM and 12 PM on Friday, to discuss the progress of the project. A weekly one hour meeting with Professor Dickerson will be held on Wednesdays from 11:00 AM until noon; during this time we will discuss research milestones plan work for the week. This project will involve approximately 25-30 work hours per week, for 4.0 Hours of Credit.